Research Article

Ultrasound-Assisted Liquid Antisolvent Method Enables Rapid Synthesis of Bioactive Nanocurcumin

Anitarakhmi Handaratri, Siti Fatimah, Bramantyo Airlangga, Firman Kurniawansyah and Sumarno*
Chemical Engineering Department, Institut Teknologi Sepuluh Nopember (ITS), Surabaya, Indonesia

* Corresponding author. E-mail: onramus@chem-eng.its.ac.id DOI: 10.14416/j.asep.2026.01.005
Received: 5 August 2025; Revised: 30 September 2025; Accepted: 30 October 2025; Published online: 12 January 2026

Abstract
Curcumin, a bioactive compound derived from turmeric, has significant pharmacological potential but suffers from poor aqueous solubility (<10 μg/mL) and low bioavailability. To overcome these limitations, this study introduces a one-step ultrasound-assisted liquid antisolvent (UALA) precipitation method, integrating simultaneous sonication during solvent–antisolvent mixing to promote rapid nucleation and suppress particle aggregation. The method reduced particle size from >1000 nm to 255 nm (76% reduction), accompanied by a decrease in crystallinity from 58.7% to 21% and a reduction in enthalpy of fusion from 442.61 to 28.57 kJ/mol (93% decrease), indicating partial amorphization. Dissolution was markedly enhanced, achieving 94.36% release within 60 min, compared with only 7.75% for raw curcumin. Antioxidant activity improved significantly, with IC_{50} values decreasing from 15 mg/mL (without sonication) to <1 mg/mL after optimized sonication, representing more than a 15-fold increase in potency. Collectively, these findings demonstrate that the UALA method provides a sustainable, carrier-free, and efficient route to produce nanocurcumin with superior physicochemical and bioactive properties, suitable for advanced pharmaceutical applications.

Keywords: Antisolvent precipitation, Bioavailability, Curcumin, Nanocurcumin, Ultrasound-assisted process

1 Introduction

Due to its inadequate solubility in water (1–10 μg/mL), curcumin, a compound derived from turmeric, has minimal bioavailability [1], [2]. Harnessing the potent biological activities of curcumin, nanocurcumin production can be used to overcome its natural solubility and bioavailability limitations [3], [4]. The heightened solubility of curcumin leads to improved bioavailability and stability, resulting in enhanced therapeutic effects. Curcumin has been found to improve the healing rate of gastric ulcers, possess anti–cancer properties, and provide anti-inflammatory and anti–aging effects [5]– [8].

Research has revealed that heating, encapsulation in nanoparticles, formation of complexes with cyclodextrins, polymorphic structure adoption, and cocrystal creation could elevate curcumin's water solubility from 0.6 μg/mL to 7.4 μg/mL, marking a 12-fold increase [9], [10]. Various techniques, including solution crystallization, slurry methods, high–speed crystallization, spray–drying, spray–chilling/ cooling, co-crystallization, emulsification, and coacervation complexes, are predominantly employed in the food industry to enhance curcumin's solubility and stability [11]–[15]. Curcumin encapsulation within liposomes, chitosan, complexing with cyclodextrins, or nanogels, has been documented. However, the issues of biocompatibility and potential safety and toxicity related to colloidal nanocarriers require careful consideration due to the possible risk of inducing diseases [16]–[19]. One appealing approach is to process the active ingredient into a nanosuspension consisting of nanoparticles entirely composed of active molecules, thereby eliminating the need for carrier materials. This nanosuspension can be used to improve the dissolution process of active ingredients with poor water solubility or permeability, ultimately accelerating the dissolution rate and enhancing the oral bioavailability of the compounds [20].

Liquid antisolvent (LAS) precipitation is a versatile bottom–up approach for producing ultrafine

particles, particularly for challenging to poorly water–soluble drugs. This straightforward technique involves adding a non–solvent to an organic solution, inducing supersaturation, and ultimately precipitation [21]. However, this bottom–up method surpasses top–down approaches by yielding nano/microstructures with fewer defects and superior molecular order. Furthermore, its practicality under ambient conditions, without the need for expensive equipment, makes it a popular choice for enhancing the dissolution rate of poorly soluble drugs [22]. To further optimize the process, sonication can be incorporated to promote rapid mixing, minimize particle agglomeration, and facilitate the formation of smaller, more uniform particles. By carefully controlling sonication parameters such as power, time, and temperature, researchers can fine–tune the properties of the resulting nanoparticles [23]. Additionally, solvent temperature plays a crucial role in modulating the reaction kinetics and phase behavior, significantly affecting the overall quality of the nanoparticles [24], [25].

Recent studies have explored carrier–free nanocurcumin preparation. For instance, Hettiarachchi *et al*., produced amorphous nanoparticles with improved dispersibility using a liquid antisolvent (LAS) method combined with sonication [26]. Although effective, their multi–step process could lead to inconsistencies in particle size and crystallinity. Similarly, Patil *et al*., employed ultrasound-assisted curcuminoid extraction followed by anti-solvent precipitation, focusing on high yield rather than nanoparticle engineering or bioavailability [27]. This work aims to develop a single–step ultrasound–assisted LAS method that directly integrates sonication with solvent–antisolvent interaction, enabling real–time nucleation, improved molecular dispersion, and reduced aggregation. By addressing the limitations of previous approaches, this study seeks to produce more uniform nanocurcumin with enhanced crystallinity, dispersibility, and potential bioavailability.

Kinetic modeling was employed to better understand and optimize nanoparticle formation. While models such as Weibull and first– or second–order kinetics have been used to describe particle size reduction and stabilization, the Peleg model—a semi-empirical approach assuming an initial fast phase followed by a slower one—was specifically applied to evaluate the effect of sonication time on curcumin concentration and yield [28], [29]. Although the Peleg model has been primarily used for curcuminoid extraction, its application here to nanoparticle formation offers a practical framework to link kinetic analysis with nanocurcumin engineering and dissolution behavior.

The effects of mixing rate, sonication time, and dichloromethane temperature (T DCM) on nanocurcumin were investigated by measuring the concentration, yield, and dissolution. The physicochemical properties of the resulting nanocurcumin were characterized using Fourier transform infrared spectroscopy (FTIR) and X–ray diffraction (XRD) to assess molecular interactions and crystallinity, differential scanning calorimetry (DSC) to examine thermal transitions, thermogravimetric analysis (TGA) to evaluate thermal stability, and particle size analysis to determine size distribution. The morphology of the nanocurcumin powder was observed through scanning electron microscopy (SEM), providing complementary insight into the particle shape and surface features.

2 Materials and Methods

2.1 *Materials*

In this study, curcumin with a purity level of 97%, obtained from Herbs Village in New Delhi, India, served as the main ingredient. No pretreatment was applied to the curcumin before use. The solvent for the curcumin was dichloromethane p.a., purchased from Merck. Double–distilled pure water (Onemed, Indonesia) was used as an antisolvent. The hydrochloric acid buffer (potassium hydrogen and hydrochloric acid) for dissolution was purchased from Sigma Aldrich.

2.2 *Experimental apparatus*

Experiments were conducted with a combination of sonication and solvent–antisolvent methods. A curcumin solution was prepared in advance by dissolving 300 mg of curcumin in 60 mL of DCM at a preserved temperature (10–30 °C). A 08895–34 model 100 W (42 kHz 6%) Cole-Parmer ultrasonic bath (Illinois, USA) and a customizable mixer (JJ–1 Fixed Time Power Mixer, China) were utilized for the process. The ultrasonic bath was equipped with a beaker glass with a maximum volume of 300 ml. The rotation speed of the mixer ranged from 800 to 1200 rpm, and the injection speed of the peristaltic pump (Kamoer, Shanghai, China) was set to 0.2 mL/min for a duration of one minute. The curcumin solution was injected into the beaker glass, which contained 100

mL of bi-distilled water at 50 °C, using the peristaltic pump. The mixer motor and ultrasonic wave were operated at the same time (0–40 min). Once finished, the sample was centrifuged at 7,155 × g (Fisher Scientific Company, Serial/Catalog number: 3456/4–970–1) for 30 min, separated from the supernatant. A comparative study was conducted to assess the impact of sonication on H+ formation. The control experiments were performed under identical conditions (T DCM 10 and 30 °C, 1000 rpm mixing) and without sonication. H+ concentration was quantified using an Eutech Instruments pH meter (model 300/310).

2.3 *Estimation of nanocurcumin concentrations*

The concentration of dispersed nanocurcumin was measured using the method reported by Som *et al*., [26]. Ten milligrams of unprocessed curcumin were mixed with 10 mL of distilled water and shaken continuously for 24 h at room temperature. The suspension was centrifuged for 30 min, and the undissolved curcumin was removed using a 0.45 mm membrane filter. The absorbance of the dispersed nanocurcumin solution was then measured at 425 nm using a UV-Vis spectrophotometer (model N4S, West Tune, China). From the calibration curve, which ranged from 1 to 10 μg/ml, a linear regression value of 0.9828 was derived. The equation for this linear regression was y = 0.005x + 0.0091. In a similar process, 10 mg of processed curcumin was dissolved in 10 mL of distilled water, and its concentration was determined using the calibration curve.

2.4 *Kinetic modelling*

In this study, the Peleg model was specifically applied to evaluate the effect of sonication time on curcumin concentration and yield, as this parameter is directly time dependent. Other process variables, such as mixing rate and solvent temperature, were not modeled using the Peleg approach, but rather treated as supporting process conditions. The generalized Peleg equation for the yield or concentration is:

$$C_t = C_0 + \frac{t}{k_1 + k_2 t} \quad (1)$$

In Equation (1), C_t is the nanocurcumin concentration at time t, k_1 is the rate constant, and k_2 is the capacity constant. Because a fresh solvent is used, the initial nanocurcumin concentration (C_0) is zero [27]. For this system, the equation was simplified as shown in Equation (2):

$$C_t = \frac{t}{k_1 + k_2 t} \quad (2)$$

2.5 *Product characterization*

The physicochemical characteristics of curcumin were comprehensively analyzed using spectroscopic, morphological, thermal, and particle sizing techniques. Fourier Transform Infrared (FTIR) spectroscopy was conducted using a PerkinElmer Spectrum 100 ATR/FTIR spectrophotometer equipped with a diamond crystal reflector. Samples were scanned four times across the 4000–500 cm^{-1} range at a resolution of 4 cm^{-1}, and spectral data were processed using Spectrum software. Crystallinity was examined by X-ray diffraction (XRD) using a Malvern Panalytical diffractometer (UK) within a 2θ range of 5–60°. The diffractograms were smoothed using the Savitzky–Golay method in Origin Pro–2018 (first–degree polynomial), and the relative crystallinity degree (RCD) was calculated as the ratio of crystalline area (A_C) to total area (A_T), using the formula in Equation (3):

$$RCD = \frac{A_C}{A_T}\, x\, 100\% \quad (3)$$

Surface morphology was observed via scanning electron microscopy (SEM) using a Zeiss Evo MA–10 microscope (Jena, Germany) operated at 8 kV with a magnification of 1000×. Prior to analysis, the samples were gold-coated to enhance conductivity. Particle size distribution of the nanoparticle was determined using a Malvern Panalytical particle size analyzer, with measurements performed at 25 ± 0.1 °C, based on the refractive index of the suspension medium. Thermal behavior and stability of curcumin were evaluated using thermogravimetric analysis (TGA) and differential scanning calorimetry (DSC) via a Simultaneous Thermal Analyzer (Mettler Toledo, Switzerland). The study was carried out over a temperature range of 25 to 500 °C at a heating rate of 20 °C/min under a nitrogen flow of 10 ml/min.

2.6 *Dissolution test*

Curcumin particle dissolution was measured using a USP apparatus type II paddle method (Electrolab TDT–08L, India). Each 5 mg of unprocessed and processed curcumin particles was added to 500 mL of

hydrochloric acid buffer (pH = 1,2), and then mixed at 50 rpm, 37 °C to simulate gastric conditions. The absorbance of 5 mL samples was recorded at 5, 10, 20, 30, 45, 60, 90, and 120 min at 425 nm using the same UV-Vis spectrophotometer. The percentage of drug dissolution at a specific time was calculated according to Equation (4):

$$\text{Dissolution (\%)} = \frac{C_t \times V}{D} \times 100\% \quad (4)$$

where C_t is the drug concentration in the dissolution medium at time t (mg/mL), V is the volume of the dissolution medium (ml), and D is the initial drug dose used in the formulation (mg).

2.7 *Antioxidant activity*

Antioxidant activity was evaluated using DPPH radical scavenging assays to determine the sample's ability to neutralize free radicals [28]. In the DPPH assay, 2 mL of DPPH solution (200 µM in ethanol) was mixed with 2 mL of the sample solution. The mixture was incubated at room temperature in the dark for 30 minutes. Absorbance was then measured at 525 nm using a UV-Vis spectrophotometer. A solution of DPPH and water served as the control, while ethanol was used as the blank. The free radical scavenging activity, where a lower absorbance value indicates higher antioxidant potential, was calculated using Equation (5):

$$\text{DPPH Scavenging (\%)} = \left(1 - \frac{A_{sample} - A_{control}}{A_{blank}}\right) \times 100 \quad (5)$$

3 Results and Discussion

3.1 *Effects of a single variable on curcumin yield and concentration in water*

Figure 1 shows the kinetics of nanocurcumin concentration and yield fitted with the Peleg model, which captures a clear biphasic behavior: a rapid initial rise followed by a slower approach to equilibrium. For concentration (blue curve), the high initial rate constant (k_1 = 4.350) corresponds to the steep early increase driven by cavitation-induced aggregate disruption and enhanced mass transfer, whereas the capacity constant (k_2 = 0.118) governs the deceleration and eventual flattening as saturation is approached. Yield (red curve) follows a similar but slower trend (k_1= 0.011; k_2 = 0.0097), consistent with progressive nucleation and particle growth; both responses reach near-steady values after 30 min. The excellent goodness-of-fit ($R^2 > 0.98$) supports the Peleg model's suitability not only as a kinetic descriptor but also as a mechanistic link between sonication dynamics and nanoparticle formation. Notably, no visible precipitation was observed and the suspensions remained homogeneously dispersed, implying colloidal stabilization via steric hindrance, surface-charge repulsion and hydration shells.

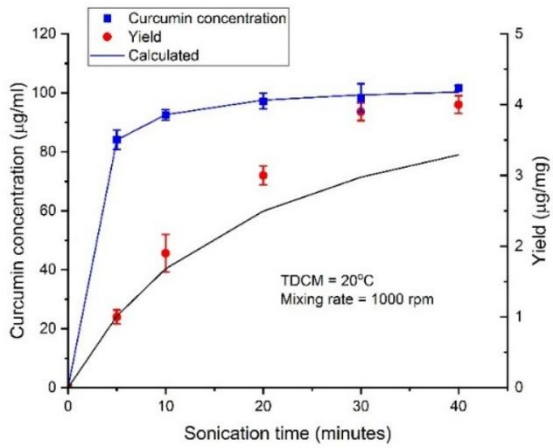

Figure 1: Peleg model fitting of curcumin dispersion as a function of sonication time, showing its effect on concentration and yield.

As shown in Figure 2(a), sonication increased curcumin concentration from 40 µg/ml under static conditions to a maximum at 1000 rpm, consistent with enhanced solvent–antisolvent transfer and nucleation reported previously [32], [33]. At higher rates, turbulence promoted particle collisions and aggregation, reducing concentration despite ongoing nucleation [34]. Yield, however, rose continuously to 1200 rpm, reflecting greater precipitation. This trade–off, also noted qualitatively in earlier studies [35], highlights 1000 rpm as the optimum balance. Without sonication (Figure 2(b)), both concentration and yield remained much lower, underscoring ultrasound's critical role in achieving stable, high–recovery suspensions.

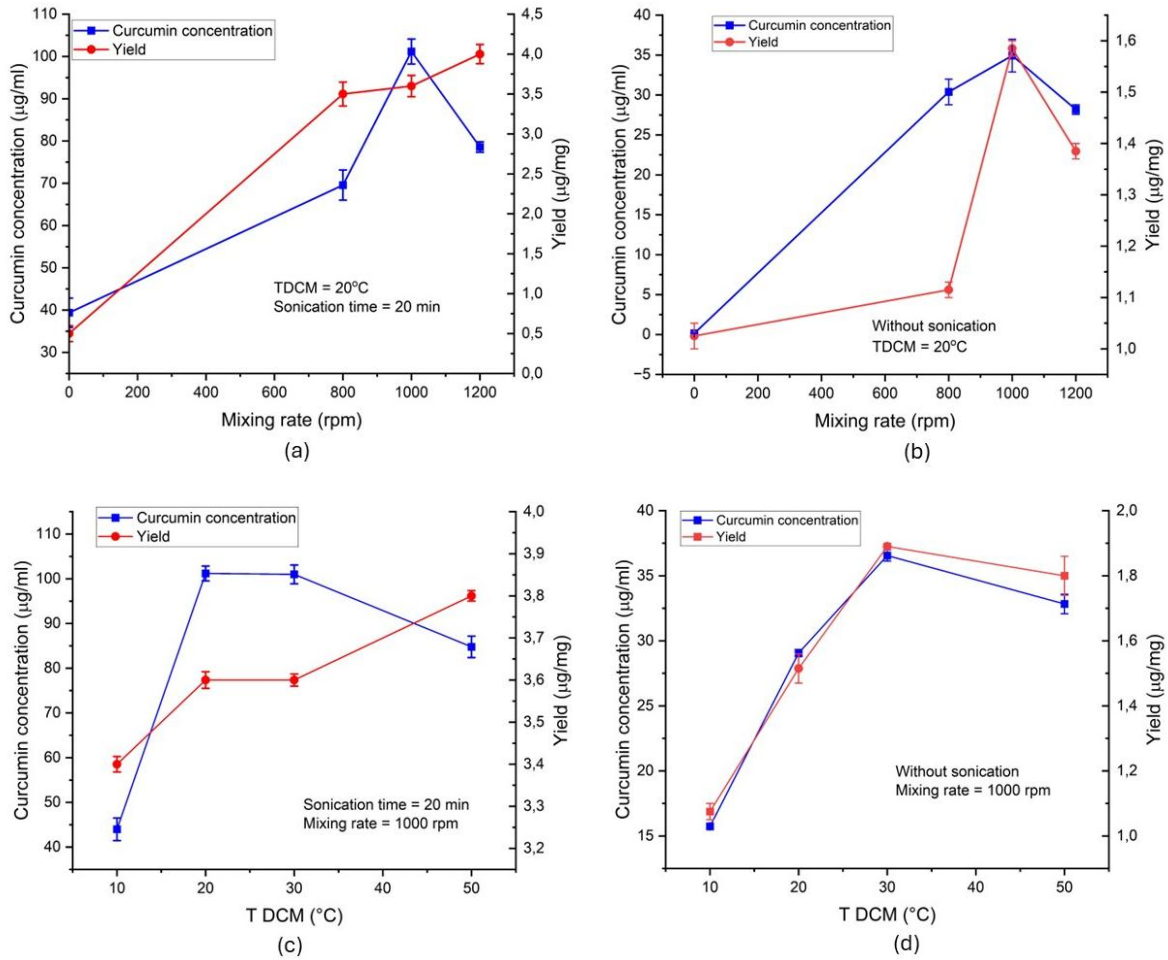

Figure 2: Effect of process variables on curcumin concentration and yield: mixing rate with sonication (a), mixing rate without sonication (b), DCM temperature with sonication, and (c) DCM temperature without sonication (d).

Preheating the DCM phase (Figure 2(c)) further modulated dispersion. With sonication, concentration rose from 44 µg/mL at 10 °C to 100 µg/mL at 20–30 °C, then declined at 50 °C, where excessive T DCM likely induced degradation or aggregation during transfer. Yield increased steadily (3.4 to 3.8 µg/mg), consistent with diffusion-driven precipitation [36]. Thus, moderate heating improved dispersion, whereas overheating compromised stability. Without sonication (Figure 2(d)), both metrics were significantly lower (≤35 µg/ml; <1.9 µg/mg), confirming that ultrasound, unlike thermal acceleration alone, sustains colloidal stability. The present work, therefore, clarifies, in contrast to prior studies that examined mixing or temperature in isolation, the mechanistic role of cavitation in suppressing aggregation and maintaining nanoparticle dispersions.

3.2 *FTIR analysis*

The infrared absorption peaks of curcumin before and after processing were analyzed, as presented in Figure 3. The peak positions and shapes of all the samples are essentially the same, indicating no significant changes. Fourier–Transform Infrared (FTIR) spectra of unprocessed and processed curcumin were scanned between 4000–650 cm^{-1}. The obtained wavelengths corresponded to the vibration of each functional group present in unprocessed and processed curcumin.

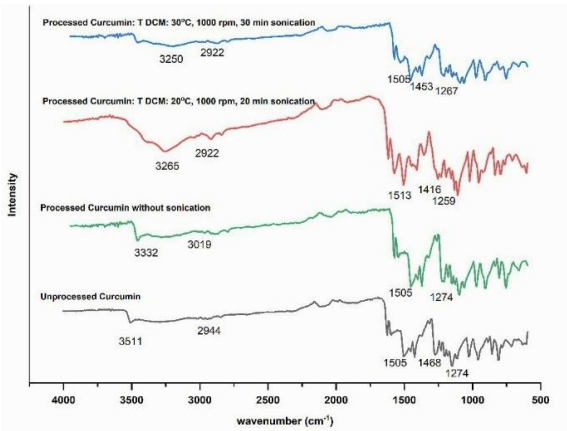

Figure 3: FTIR Spectra of unprocessed and processed curcumin.

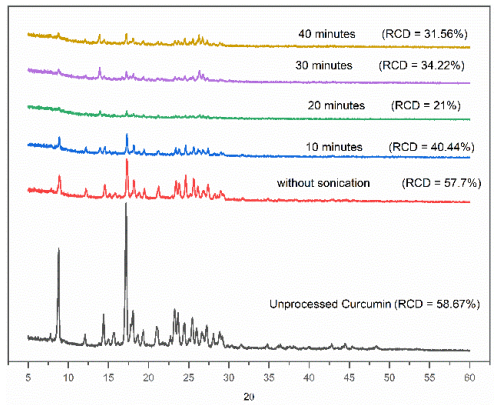

Figure 4: XRD Analysis of unprocessed and processed curcumin (T DCM: 30 °C, mixing rate: 1000rpm).

The results show that the O-H peak at 3511 cm^{-1} in raw curcumin shifted to 3332 cm^{-1}, 3265 cm^{-1}, and 3250 cm^{-1} in processed curcumin, indicating hydrogen interaction and molecular conformation changes. The reduction in curcumin particle size exposes individual OH groups, promoting hydrogen bond formation with water molecules. This enhanced intermolecular interaction, coupled with the decreased intensity of the –OH peak, suggests reduced intramolecular hydrogen bonding within the curcumin structure, further facilitating water interaction[37].

The aliphatic C–H vibration remained constant at around 2922 cm^{-1} in all spectra. The C=C and C–H vibrations in the aromatic ring of curcumin at 1505 cm^{-1} and 1468 cm^{-1} became sharper and more intense at 1513 cm^{-1} and 1416 cm^{-1} in processed curcumin, respectively. This suggests that the chemical environment or conformation of specific functional groups changed after mixing. Processed curcumin molecules were more likely to be predisposed to forming hydrogen bonds with water molecules instead of each other, thereby increasing curcumin's dispersity in water through new hydrogen bond formations.

Other curcumin formulations have shown similar O–H stretching band shifts, where particle size reduction or encapsulation tends to enhance hydrogen bonding with the environment instead of altering the molecule's core structure. Hettiarachchi *et al*., reported a broadened, red–shifted hydroxyl peak in ultrasound–prepared nanocurcumin, and Kanwal *et al*., described comparable FTIR changes in curcumin nanoparticles—both pointing to stronger intermolecular interactions [2], [38].

3.3 *XRD Analysis*

A lower degree of crystallinity is indicated by the reduced peak intensities in the XRD spectra of the processed samples, as shown in Figure 4, compared to those of unprocessed curcumin. With increasing sonication time, the crystallinity of curcumin decreased, leading to broadened peaks and reduced peak intensities. The degree of crystallinity (RCD) of unprocessed curcumin was 58.67%. On the other hand, the RCD values of curcumin processed under sonication at a T DCM of 30°C and a mixing rate of 1000 rpm for 10, 20, 30, and 40 minutes were 40.44%, 21%, 34.22%, and 31.56%, respectively. The RCD for the sample without sonication was 57.70%. The most notable anomaly was observed in the 20-minute sonication sample, where the peaks were broad and less intense, indicating a substantial reduction in crystallinity and potential formation of amorphous regions. Type–I crystal forms of curcumin were observed in all samples (at 2θ = 17–18°). The analysis of processed curcumin samples proved the presence of type–II or type–III crystal forms (orthorhombic), which were specified by peaks at 2θ signals of 8–9°, 14–15°, and 26–27° [39].

Due to weaker hydrogen bonds, the orthorhombic crystals have a higher solubility and faster release rate in aqueous solution compared to type–I crystals [40]. This aligns with the analysis results, which show that the concentration of processed curcumin in water was 3–10 times higher than the initial concentration of curcumin soluble in water. Rhombohedral crystals of curcumin often appear when the hydrogen bonding interactions between curcumin molecules are disrupted [41]. The

carbonyl group (C=O) in the orthorhombic structure exhibits higher polarity, facilitating better interaction with water. This fact provides evidence that the LAS method under ultrasonic conditions can overcome the relatively higher nucleation barrier of the monoclinic form.

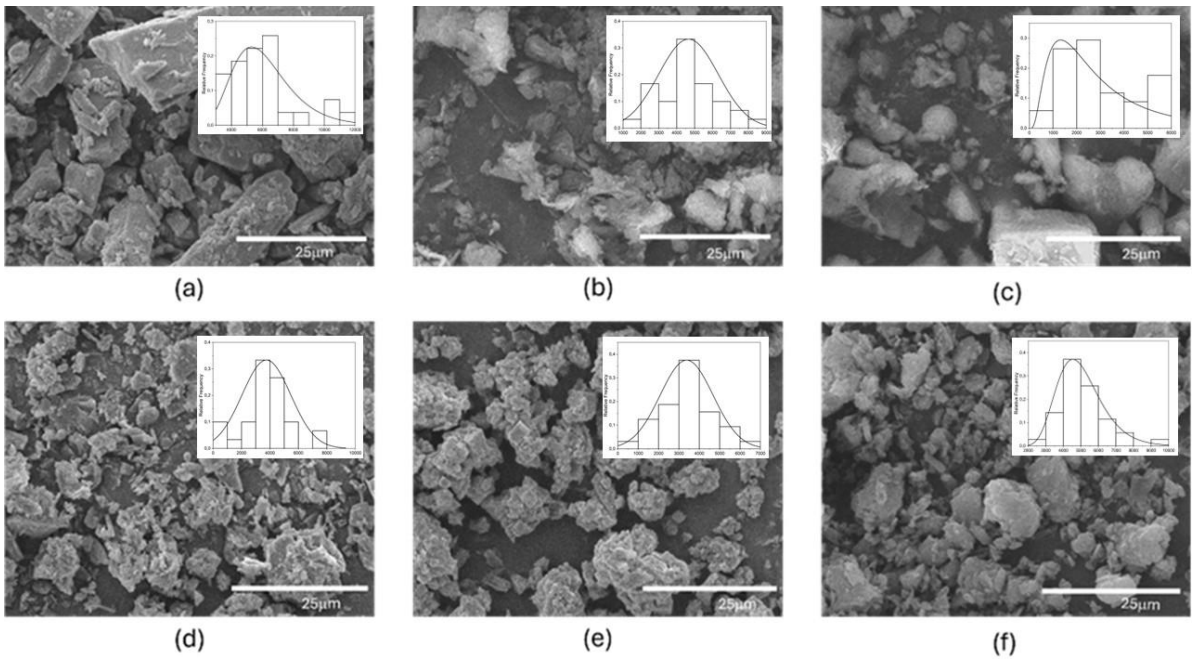

Figure 5: SEM Images of unprocessed curcumin (a) and curcumin processed with DCM at 30 °C and 1000 rpm without sonication (b) and with sonication for 10 min (c), 20 min (d), 30 min (e), and 40 min (f).

3.4 *Curcumin morphology*

The SEM results for each variable are presented in Figure 5. It was observed that the crystals of unprocessed curcumin (Figure 5a) appeared relatively large and well-defined, indicating a high degree of crystallinity. The edges were sharp, and the surface was relatively smooth. In the process without sonication (Figure 5(b)), curcumin particles looked bulkier and more irregular, with a great degree of agglomeration. The particles seemed smaller, with more fragments broken during the 10-minute sonication process (Figure 5(c)). This shift might prove that sonication had broken down particle aggregates into smaller sizes and altered their crystal shape. This process might also have enlarged the particle surface area due to the formation of particles in smaller sizes.

Additionally, significant morphological differences were observed in the 10– and 20–min sonication samples (Figure 5(d)). The surface of the particles appears rougher and smaller, which suggests that longer sonication time amplifies energy in the system and leads to further deformation. Based on the XRD analysis, curcumin sonicated for 20 minutes exhibited a reduction in crystallinity to half that of unprocessed curcumin. Overall, the particles resemble fragments in shape, with a few elongated forms characteristic of the combination of monoclinic (I) and orthorhombic (II and III) forms [39]. However, some small particle aggregation occurred during the 30-minute ultrasonic contact (Figure 5(e)). At this stage, the energy from sonication caused the particles to collide and agglomerate, forming larger clusters. This agglomeration occurred because the adhesive forces between particles became dominant.

Re-agglomeration might have happened in the curcumin solution after 40 min of sonication (Figure 5(f)) when the system was not given enough mechanical energy to keep the curcumin particles dispersed. The surface characteristics of a nanoparticle, such as the zeta potential (surface charge) characteristic, can be altered by extended sonication, which has an impact on colloidal stability [42].

To address the apparent discrepancy between SEM morphology and particle size analysis, size distributions were extracted directly from SEM images and are presented as inset histograms in Figure 5. These

histograms reveal that, although the SEM micrographs visually suggest broad size variation, most particles actually fall within a relatively narrow range, yielding unimodal distributions centered near the mean. Consequently, the particle size analysis returned low standard deviation values, as larger or irregular particles constituted only a minor fraction.

3.5 *Particle size distribution*

As shown in Figure 6, the unprocessed curcumin exhibited the largest particle size, averaging 1065.72 nm with a standard deviation of 137.00 nm. This value was significantly higher (p-value < 0.05) than all other treatments, as indicated by the distinct grouping (letter "a"). Upon processing using the liquid antisolvent (LAS) method, a substantial reduction in particle size was observed. The sample prepared without sonication showed a mean particle size of 442.95 nm, while samples subjected to sonication for 10 to 40 min ranged between 255.08 and 338.68 nm. Despite the numerical trend indicating a progressive decrease in particle size with increasing sonication time, all processed samples—including those with and without sonication—were statistically grouped under the same category (letter "b"), indicating no significant difference among them. Notably, the smallest particle size (255.08 nm) and lowest standard deviation (8.24 nm) were achieved at 20 and 40 min of sonication, suggesting improved uniformity and particle stability. These results imply that the LAS method alone is sufficient to induce nanoscale particle formation, and while sonication enhances particle dispersion and reduces variability, it does not result in a statistically significant further reduction in size.

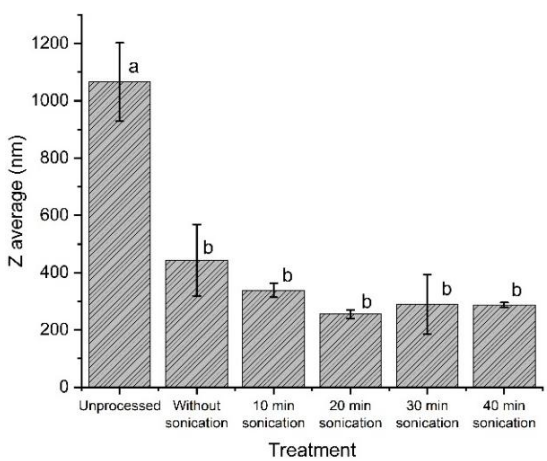

Figure 6: Particle size of curcumin (mean±SD, n=3).

Previous studies using a multi-step approach have reported smaller curcumin particles [12], [38], [43]. In our work, the one-step UALA method yielded slightly larger sizes (255–338 nm); however, the particles exhibited narrow distributions and good uniformity. The difference can be attributed to the integrated nature of the UALA process, where size reduction and precipitation occur simultaneously, without a separate secondary step that could further decrease particle size. This indicates that while the absolute size is somewhat larger, the one–step method effectively ensures nanoscale formation with enhanced dispersion stability.

3.6 *Thermal analysis*

The modifications in the physical characteristics of curcumin significantly influenced its thermal behaviour, as revealed through DSC (Figure 7) and TGA (Figure 8) analysis of the curcumin powder obtained from processing at 1000 rpm for 30 min at 30 °C. DSC thermograms corroborated these findings. Unprocessed curcumin exhibited two distinct endothermic peaks at 29.19 °C and 178.21 °C, corresponding to the loss of surface–bound volatiles and the melting of its crystalline phase, respectively. In contrast, the processed curcumin displayed a single, broader endothermic peak at 176.49 °C with markedly reduced intensity. The enthalpy of fusion decreased substantially from 442.61 kJ/mol in the unprocessed sample to 28.57 kJ/mol after processing, reflecting the disruption of long–range crystalline order and the formation of an amorphous or partially amorphous structure [41], [44].

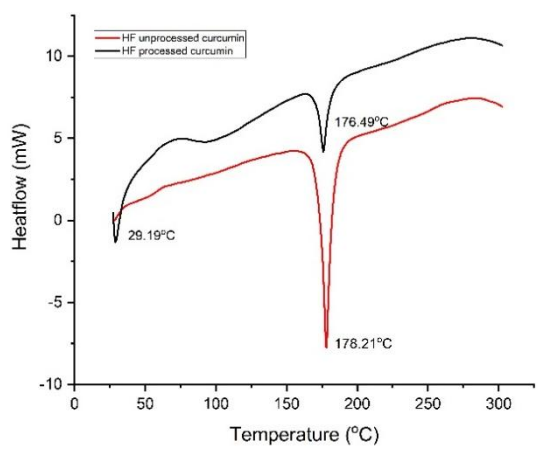

Figure 7: DSC Analysis of curcumin samples.

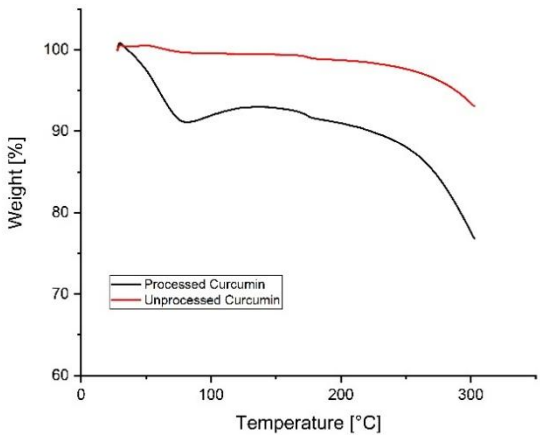

Figure 8: TGA Analysis of curcumin samples.

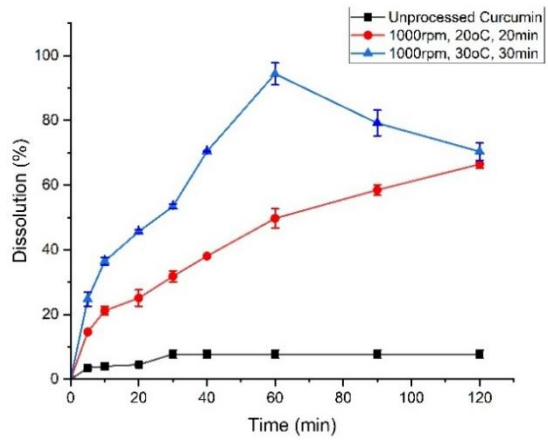

Figure 9: Dissolution test of unprocessed and processed curcumin (mean ± SD, n=3).

The TGA profile of processed curcumin exhibited distinct differences from that of the unprocessed material. An initial mass loss of 7.38% observed in the 40–100 °C range is attributed to the release of moisture or loosely bound volatile components. This suggests enhanced interaction between the processed curcumin particles and the aqueous medium, likely facilitated by the increase in surface area. A further mass loss of 6.46% between 100–220 °C indicates that the processed sample undergoes earlier decomposition than the unprocessed counterpart, consistent with a reduction in thermal stability typically associated with increased amorphous content. Beyond 220 °C, the rate of mass loss was slower compared to unprocessed curcumin, suggesting that the remaining components after the initial decomposition exhibit relatively higher thermal stability.

All thermal transitions observed were endothermic in nature, indicating that energy input was required for both melting and phase transformation processes. The downward shift and broadening of the melting peak, alongside the substantial enthalpy reduction, were observed after ultrasonic-enhanced LAS processing of curcumin. As reported by Bagale *et al*., and Ahlawat *et al*., similar thermal transitions—marked by a downward shift in melting point, peak broadening, and reduced enthalpy—are strongly suggestive of altered thermal behavior and are consistent with structural modifications in the crystalline phase of curcumin [45], [46].

3.7 *Dissolution test*

As depicted in Figure 9, the application of ultrasound led to a pronounced increase in curcumin dissolution compared with the unprocessed, where the most significant effect was observed under the condition of 30 °C for 30 min at 1000 rpm. Under these conditions, dissolution peaked within the first hour (nearly complete release), which is substantially higher than the levels typically achieved by antisolvent or micronization methods [47], [48].

When compared with other curcumin formulations, the advantages of the UALA process are evident. Co–amorphous systems or cocrystals often require co–formers [49], [50], and nanocrystals stabilized with proteins or polysaccharides rely on external stabilizers [51]. In contrast, the present carrier-free UALA approach achieved rapid and extensive dissolution (94% at 60 min), underscoring both efficiency and simplicity. The subsequent decline after 60 min resembles the “spring–parachute” effect described in other curcumin nano formulations, typically attributed to re–aggregation or recrystallization within the dissolution medium.

3.8 *Antioxidant analysis*

As presented in Table 1, the combination of mixing rate and sonication time significantly influenced the IC_{50} values of curcumin. Lower IC_{50} values indicate enhanced antioxidant activity, which is closely associated with improved curcumin dissolution and dispersion. At a mixing rate of 800 rpm without sonication, the IC_{50} remained relatively high (14.94±0.27 mg/mL), reflecting the inherent poor

solubility of raw curcumin. The application of sonication progressively reduced the IC_{50}, with noticeable improvements observed after 10 min (9.28±0.22 mg/mL) and 20 min (7.28±0.12 mg/mL). At 30 min, the IC_{50} dropped sharply to below 1 mg/mL, indicating a substantial enhancement in dissolution. However, extending the sonication to 40 min did not yield a statistically significant difference, suggesting that the optimal duration had been reached.

Table 1: Antioxidant analysis of processed curcumin.

Mixing Rate (rpm)	Sonication Time (min)	IC_{50} (mg/mL)
800	0	14.94±0.27
	5	13.64±0.20
	10	9.28±0.22
	20	7.28±0.12
	30	<1
	40	<1
1000	0	14.99±0.01
	5	14.59±0.26
	10	14.34±0.47
	20	6.62±0.33
	30	<1
	40	11.23±0.36
1200	0	15.60±0.31
	5	6.43±0.06
	10	5.76±0.04
	20	<1
	30	<1
	40	<1

At a mixing rate of 1000 rpm, the IC_{50} without sonication was similarly high (14.99±0.01 mg/mL), and up to 10 min of sonication had minimal effect, with values remaining above 14 mg/mL. A significant reduction occurred at 20 min (6.62±0.33 mg/mL), with the lowest IC_{50} observed at 30 min (<1 mg/mL). Interestingly, a slight increase in IC_{50} to 11.23±0.36 mg/mL was recorded at 40 min, possibly indicating degradation or changes in curcumin structure due to prolonged sonication.

In contrast, at a mixing rate of 1200 rpm, the IC_{50} value without sonication was the highest among all conditions (15.60±0.31 mg/mL), suggesting that increasing the mixing rate alone was insufficient to enhance curcumin solubility. Nevertheless, sonication for 5 and 10 min led to a significant improvement, reducing IC_{50} to 6.43±0.08 and 5.73±0.04 mg/mL, respectively. A further decrease to below 1 mg/mL occurred at 20 min and was maintained through 40 minutes, indicating enhanced stability and dispersion of curcumin under high mixing and moderate sonication conditions.

3.9 *The nanocurcumin formation process*

Figure 10 illustrates that the ultrasonic-assisted liquid antisolvent (LAS) technique successfully produced stable nanocurcumin particles with uniform dispersion and enhanced physicochemical properties. This outcome resulted from the synergistic effects of antisolvent precipitation and ultrasonic cavitation. Upon injection of curcumin–dichloromethane (DCM) solution into water, a strong supersaturation gradient was generated due to the low solubility of curcumin in the aqueous phase.

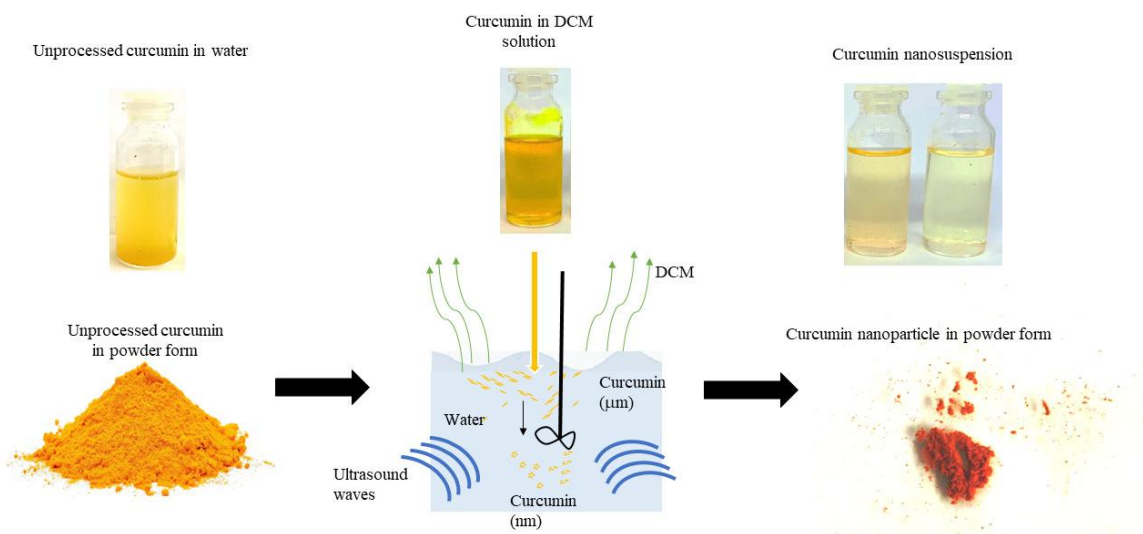

Figure 10: Schematic illustration of a stable curcumin nanoparticle obtained using ultrasonically enhanced LAS.

Rapid mixing, assisted by controlled stirring and ultrasound, promoted homogeneous blending of the solvent and antisolvent phases, thereby facilitating uniform nucleation while preventing uncontrolled agglomeration. Concurrently, the high volatility of DCM allowed its rapid evaporation in hot water (50 °C), leading to curcumin precipitation and dispersion in nanoscale form. Without ultrasonic irradiation, these particles would readily aggregate because of the intrinsic hydrophobicity of curcumin; however, sonication ensured stable dispersion in aqueous media [52].

At the mechanistic level, ultrasound contributed through two interconnected processes. First, micro–convection induced by acoustic oscillations enhanced localized supersaturation and accelerated molecular transport toward crystal nuclei. This turbulence simultaneously disrupted anisotropic crystal growth, resulting in reduced crystallinity and the frequent appearance of amorphous or semi–crystalline nanocurcumin [53]. Second, cavitation collapse generated intense shear forces and shock waves that fragmented pre–existing nuclei, creating multiple secondary nucleation sites. Localized zones of high supersaturation around collapsing bubbles further amplified nucleation events, yielding a large population of small nuclei that grew into nanosized particles with reduced crystallinity [54]. Collectively, these mechanisms explain the simultaneous improvements in particle size control, dispersion stability, and aqueous compatibility.

The mechanisms observed here are consistent with previous reports on ultrasound–assisted nanomaterial synthesis. For instance, Español *et. al.,* demonstrated that ultrasound irradiation during the biomimetic synthesis of MOF–HAp composites improved dispersion, reduced agglomeration, and yielded smaller particle sizes, ultimately enhancing catalytic performance [55]. Similarly, Hu *et. al.,* reviewed ultrasound-assisted meat curing and highlighted that cavitation-induced microjets and turbulence accelerated mass transfer and structural modification, leading to more efficient processing and improved product quality [56]. These parallels emphasize the universal role of sonication in promoting efficient mass transfer, controlling nucleation, and tailoring microstructural properties across different material systems.

4 Conclusions

This study demonstrates that ultrasound–assisted liquid antisolvent (UALA) processing can markedly enhance curcumin's aqueous solubility, dissolution rate, and antioxidant activity. The optimized conditions produced nanocurcumin with reduced particle size (255 nm), partial crystallinity, and high bioactivity (substantially lower IC_{50} values). Dissolution was significantly improved, with up to 94% release within 60 minutes compared with only 7% for raw curcumin. However, a decline in dissolved curcumin at longer time points indicates possible reaggregation or recrystallization in the medium, underlining the need for further mechanistic investigation. Precise control of processing intensity is also crucial, as excessive sonication can promote agglomeration. Overall, the ultrasound–assisted LAS approach offers a sustainable, carrier–free, and scalable route to bioavailable nanocurcumin, making it suitable for pharmaceutical and functional food applications. Future studies should address long–term stability, in vivo performance, and time–resolved monitoring of particle size and solid–state properties during dissolution to guide the development of more stable and effective formulations

Acknowledgments

The authors wish to extend their appreciation for the funding support provided by Indonesian Education Scholarship (BPI), Center for Higher Education Funding and Assessment (PPAPT), and Indonesian Endowment Fund for Education (LPDP) for this study. BPI No. 202209091124.

Author Contributions

A.H.: Data curation, Investigation, Methodology, Formal analysis, Writing – original draft; S.F.: Data curation, Investigation; B.A.: Writing-Review & Editing; F.K.: Conceptualization, Supervision, Writing-Review & Editing; S.S.: Conceptualization, Supervision, Writing-Review & Editing.

Conflicts of Interest

The authors declare no conflict of interest.

References

[1] B. Zheng and D. J. McClements, "Formulation of more efficacious curcumin delivery systems using colloid science: Enhanced solubility, stability, and bioavailability," *Molecules*, vol.

25, no. 12, pp. 1–25, 2020, doi: 10.3390/molecules25122791.

[2] Q. Kanwal et al., "Curcumin nanoparticles: Physicochemical fabrication, characterization, antioxidant, enzyme inhibition, molecular docking and simulation studies," *RSC Advances*, vol. 13, no. 32, pp. 22268–22280, 2023, doi: 10.1039/d3ra01432k.

[3] Deepika, M. Prasad, A. Salar, and R. K. Salar, "In vitro anticancer activity of curcumin loaded chitosan nanoparticles (CLCNPs) against Vero cells," *Pharmacological Research – Modern Chinese Medicine*, vol. 3, p. 100116, 2022, doi: 10.1016/j.prmcm.2022.100116.

[4] A. Rajasekar, T. Devasena, S. Suresh, B. Senthil, R. Sivaramakrishnan, and A. Pugazhendhi, "Curcumin nanospheres and nanorods: Synthesis, characterization and anticancer activity," *Process Biochemistry*, vol. 112, pp. 248–253, 2022, doi: 10.1016/j.procbio.2021.12.007.

[5] L. Jamir, V. Kumar, J. Kaur, S. Kumar, and H. Singh, "Composition, valorization and therapeutical potential of molasses: A critical review," *Environmental Technology Reviews*, vol. 10, no. 1, pp. 131–142, 2021, doi: 10.1080/21622515.2021.1892203.

[6] M. Hegde, S. Girisa, B. BharathwajChetty, R. Vishwa, and A. B. Kunnumakkara, "Curcumin formulations for better bioavailability: What we learned from clinical trials thus far?," *ACS Omega*, vol. 8, no. 12, pp. 10713–10746, 2023, doi: 10.1021/acsomega.2c07326.

[7] S. Aghajanpour et al., "Applying liquisolid technique to enhance curcumin solubility: A central composite design study," *Chemical Papers*, 2024, doi: 10.1007/s11696-024-03741-7.

[8] D. H. Hanna and G. R. Saad, "Nanocurcumin: Preparation, characterization and cytotoxic effects towards human laryngeal cancer cells," *RSC Advances*, vol. 10, no. 35, pp. 20724–20737, 2020, doi: 10.1039/d0ra03719b.

[9] Z. Sayyar and H. Jafarizadeh-Malmiri, "Preparation of curcumin nanodispersions using subcritical water – Screening of different emulsifiers," *Chemical Engineering & Technology*, vol. 43, no. 2, pp. 263–272, 2020, doi: 10.1002/ceat.201900415.

[10] J. Górnicka, M. Mika, O. Wróblewska, P. Siudem, and K. Paradowska, "Methods to improve the solubility of curcumin from turmeric," *Life*, vol. 13, no. 1, pp. 1–13, 2023, doi: 10.3390/life13010207.

[11] W. Gu, D. Liu, and J. Sun, "Co-crystallization of curcumin for improved photodynamic inactivation of *Vibrio parahaemolyticus* and its application for the preservation of cooked clams," *International Journal of Food Microbiology*, vol. 378, p. 109816, 2022, doi: 10.1016/j.ijfoodmicro.2022.109816.

[12] I. A. Walbi et al., "Development of a curcumin-loaded lecithin/chitosan nanoparticle utilizing a Box–Behnken design of experiment: Formulation design and influence of process parameters," *Polymers (Basel)*, vol. 14, no. 18, 2022, doi: 10.3390/polym14183758.

[13] Y. Chen et al., "Design and evaluation of inhalable nanocrystals embedded microparticles with enhanced redispersibility and bioavailability for breviscapine," *Powder Technology*, vol. 377, pp. 128–138, 2021, doi: 10.1016/j.powtec.2020.08.040.

[14] L. Pudziuvelyte, A. Siauruseviciute, R. Morkuniene, R. Lazauskas, and J. Bernatoniene, "Influence of technological factors on the quality of chitosan microcapsules with *Boswellia serata L.* essential oil," *Pharmaceutics*, vol. 14, no. 6, 2022, doi: 10.3390/pharmaceutics14061259.

[15] A. Behnamnik, M. Vazifedoost, Z. Didar, and B. Hajirostamloo, "Evaluation of physicochemical, structural, and antioxidant properties of microencapsulated seed extract from *Securigera securidaca* by co-crystallization method during storage time," *Biocatalysis and Agricultural Biotechnology*, vol. 35, p. 102090, 2021, doi: 10.1016/j.bcab.2021.102090.

[16] G. K. Pamunuwa, M. Prasadani, T. U. G. Nanayakkara, and S. N. Atapattu, "Effect of liposomal encapsulation of curcumin and α-tocopherol on sensory and physicochemical properties, and retention of antioxidant capacity of fortified cookies during baking," *Food Chemistry Advances*, vol. 3, 2023, doi: 10.1016/j.focha.2023.100504.

[17] A. Bonaccorso et al., "Optimization of curcumin nanocrystals as promising strategy for nose-to-brain delivery application," *Pharmaceutics*, vol. 12, no. 5, 2020, doi: 10.3390/pharmaceutics12050476.

[18] A. M. Abdelmonem, A. Lavrentieva, and N. C. Bigall, "Fabrication of surface-functionalizable amphiphilic curcumin nanogels for biosensing and biomedical applications," *Chemical Papers*, vol. 78, no. 1, pp. 533–546, 2024, doi: 10.1007/s11696-023-03108-4.

[19] N. M. Elbaz, L. M. Tatham, A. Owen, S. Rannard, and T. O. McDonald, "Redispersible nanosuspensions as a plausible oral delivery system for curcumin," *Food Hydrocolloids*, vol. 121, p. 107005, 2021, doi: 10.1016/j.foodhyd.2021.107005.

[20] F. Sadeghi, M. Ashofteh, A. Homayouni, M. Abbaspour, A. Nokhodchi, and H. A. Garekani, "Antisolvent precipitation technique: A very promising approach to crystallize curcumin in presence of polyvinyl pyrrolidon for solubility and dissolution enhancement," *Colloids and Surfaces B: Biointerfaces*, vol. 147, pp. 258–264, 2016, doi: 10.1016/j.colsurfb.2016.08.004.

[21] A. V. Dighe, P. K. R. Podupu, P. Coliaie, and M. R. Singh, "Three-step mechanism of antisolvent crystallization," *Crystal Growth & Design*, vol. 22, no. 5, pp. 3119–3127, 2022, doi: 10.1021/acs.cgd.2c00014.

[22] J. Luo et al., "Rapid and sustainable production of nano and micro medicine crystals via freeze-dissolving technology," *Powder Technology*, vol. 443, p. 119913, 2024, doi: 10.1016/j.powtec.2024.119913.

[23] K. Araki et al., "Application of a microreactor to pharmaceutical manufacturing: Preparation of amorphous curcumin nanoparticles and controlling the crystallinity of curcumin nanoparticles by ultrasonic treatment," *AAPS PharmSciTech*, vol. 21, no. 1, pp. 1–9, 2020, doi: 10.1208/s12249-019-1418-8.

[24] P. Kanakasabai, S. Sivamani, and K. Thirumavalavan, "Box–Behnken design and analysis for liquid–liquid extraction of methyl red dye from its aqueous solution with benzene," *Chemical Papers*, vol. 77, no. 11, pp. 7225–7235, 2023, doi: 10.1007/s11696-023-03013-w.

[25] C. S. Dzah et al., "The effects of ultrasound-assisted extraction on yield, antioxidant, anticancer and antimicrobial activity of polyphenol extracts: A review," *Food Bioscience*, vol. 35, p. 100547, 2020, doi: 10.1016/j.fbio.2020.100547.

[26] S. Som et al., "Quality by design-based crystallization of curcumin using liquid antisolvent precipitation: Micromeritic, biopharmaceutical, and stability aspects," *Assay and Drug Development Technologies*, vol. 18, no. 1, pp. 11–33, 2020, doi: 10.1089/adt.2018.913.

[27] C. Tan, J. Xie, X. Zhang, J. Cai, and S. Xia, "Polysaccharide-based nanoparticles by chitosan and gum arabic polyelectrolyte complexation as carriers for curcumin," *Food Hydrocolloids*, vol. 57, pp. 236–245, 2016, doi: 10.1016/j.foodhyd.2016.01.021.

[28] Z. Wu et al., "Rational fabrication of folate-conjugated zein/soy lecithin/carboxymethyl chitosan core-shell nanoparticles for delivery of docetaxel," *ACS Omega*, vol. 7, no. 15, pp. 13371–13381, 2022, doi: 10.1021/acsomega.2c01270.

[29] N. Tshilande, L. Mammino, and M. K. Bilonda, "The study of molecules and processes in solution: An overview of questions, approaches and applications," *Computation*, vol. 12, no. 4, 2024, doi: 10.3390/computation12040078.

[30] S. Xue, J. Xu, Y. Han, J. Zhang, and W. Li, "Solvent–antisolvent competitive interactions mediate imidacloprid polymorphs in antisolvent crystallization," *Crystal Growth & Design*, vol. 21, no. 8, pp. 4318–4328, 2021, doi: 10.1021/acs.cgd.1c00070.

[31] I. Szilagyi, T. Szabo, A. Desert, G. Trefalt, T. Oncsik, and M. Borkovec, "Particle aggregation mechanisms in ionic liquids," *Physical Chemistry Chemical Physics*, vol. 16, no. 20, pp. 9515–9524, 2014, doi: 10.1039/c4cp00804a.

[32] A. Cardellini, M. Fasano, M. B. Bigdeli, E. Chiavazzo, and P. Asinari, "Thermal transport phenomena in nanoparticle suspensions," *Journal of Physics: Condensed Matter*, vol. 28, no. 48, 2016, doi: 10.1088/0953-8984/28/48/483003.

[33] Y. Wang, Z. Li, S. Fayu, F. Li, and W. Wang, "Preparation of curcumin submicron particles by supercritical antisolvent method with external adjustable annular gap nozzle," *Scientific Reports*, vol. 15, no. 1, pp. 1–17, 2025, doi: 10.1038/s41598-025-87787-x.

[34] L. Liu, C. Yao, S. Zhao, Z. Liu, and G. Chen, "Enhanced antisolvent processes in an ultrasonic capillary microreactor: Cavitation, mixing and application in mini-emulsion preparation," *Chemical Engineering Journal*, vol. 466, p. 143426, 2023, doi: 10.1016/j.cej.2023.143426.

[35] J. Liu, M. Svärd, P. Hippen, and Å. C. Rasmuson, "Solubility and crystal nucleation in organic solvents of two polymorphs of curcumin," *Journal of Pharmaceutical Sciences*, vol. 104, no. 7, pp. 2183–2189, 2015, doi: 10.1002/jps.24463.

[36] B. Niu, Z. Li, C. Luan, and B. Zhao, "The dissolution and bioavailability of curcumin reinforced by loading into porous starch under solvent evaporation," *International Journal of*

Biological Macromolecules, vol. 287, 2025, doi: 10.1016/j.ijbiomac.2024.138611.

[37] S. S. Hettiarachchi, S. P. Dunuweera, A. N. Dunuweera, and R. M. G. Rajapakse, "Synthesis of curcumin nanoparticles from raw turmeric rhizome," *ACS Omega*, vol. 6, no. 12, pp. 8246–8252, 2021, doi: 10.1021/acsomega.0c06314.

[38] C. Siebenmorgen, A. Poortinga, and P. van Rijn, "Sono-processes: Emerging systems and their applicability within the (bio-)medical field," *Ultrasonics Sonochemistry*, vol. 100, p. 106630, 2023, doi: 10.1016/j.ultsonch.2023.106630.

[39] F. Kurniawansyah, R. Mammucari, and N. R. Foster, "Polymorphism of curcumin from dense gas antisolvent precipitation," *Powder Technology*, vol. 305, pp. 748–756, 2017, doi: 10.1016/j.powtec.2016.10.067.

[40] A. A. Thorat and S. V. Dalvi, "Ultrasound-assisted modulation of concomitant polymorphism of curcumin during liquid antisolvent precipitation," *Ultrasonics Sonochemistry*, vol. 30, pp. 35–43, 2016, doi: 10.1016/j.ultsonch. 2015.11.025.

[41] S. Shome, A. Das Talukdar, S. Tewari, S. Choudhury, M. K. Bhattacharya, and H. Upadhyaya, "Conjugation of micro/nanocurcumin particles to ZnO nanoparticles changes the surface charge and hydrodynamic size thereby enhancing its antibacterial activity against *Escherichia coli* and *Staphylococcus aureus*," *Biotechnology and Applied Biochemistry*, vol. 68, no. 3, pp. 603–615, Jun. 2021, doi: 10.1002/bab.1968.

[42] R. Kumar et al., "Nanoparticle preparation of pharmaceutical compounds via wet milling: Current status and future prospects," *Powder Technology*, vol. 435, p. 119430, 2024, doi: 10.1016/j.powtec.2024.119430.

[43] M. Brycka et al., "Heat capacity and thermodynamic functions of crystalline and amorphous forms of Lovastatin," *Scientific Reports*, vol. 15, no. 1, pp. 1–12, 2025, doi: 10.1038/s41598-025-05075-0.

[44] S. Ahlawat, V. Budhwar, and M. Choudhary, "Enhancement of curcumin's physicochemical properties by developing its eutectic mixtures," *Journal of Applied Pharmaceutical Research*, vol. 12, no. 1, pp. 71–81, 2024, doi: 10.18231/j.joapr.2024.12.1.71.81.

[45] U. Bagale, A. Kadi, A. Malinin, I. Potoroko, S. Sonawane, and S. Potdar, "Ultrasound-assisted stable curcumin nanoemulsion and its application in bakery product," *International Journal of Food Science*, vol. 2022, 2022, doi: 10.1155/2022/4784794.

[46] S. Mottola and I. De Marco, "Curcumin/carrier coprecipitation by supercritical antisolvent route," *Pharmaceutics*, vol. 16, no. 3, 2024, doi: 10.3390/pharmaceutics16030352.

[47] Z. Zhao et al., "Formation of curcumin nanoparticles via solution-enhanced dispersion by supercritical CO_2," *International Journal of Nanomedicine*, vol. 10, pp. 3171–3181, 2015, doi: 10.2147/IJN.S80434.

[48] J. Han et al., "Deaggregation and crystallization inhibition by small amount of polymer addition for a co-amorphous curcumin-magnolol system," *Pharmaceutics*, vol. 13, no. 10, 2021, doi: 10.3390/pharmaceutics13101725.

[49] H. Wang et al., "Improving the dissolution rate and bioavailability of curcumin via co-crystallization," *Pharmaceuticals*, vol. 17, no. 4, 2024, doi: 10.3390/ph17040489.

[50] D. Yang et al., "Construction, characterization and bioactivity evaluation of curcumin nanocrystals with extremely high solubility and dispersion prepared by ultrasound-assisted method," *Ultrasonics Sonochemistry*, vol. 104, p. 106835, 2024, doi: 10.1016/j.ultsonch.2024. 106835.

[51] Vikash and V. Kumar, "Ultrasonic-assisted de-agglomeration and power draw characterization of silica nanoparticles," *Ultrasonics Sonochemistry*, vol. 65, p. 105061, 2020, doi: 10.1016/j.ultsonch. 2020.105061.

[52] R. Kumar, A. K. Thakur, N. Banerjee, A. Kumar, G. K. Gaurav, and R. K. Arya, "Liquid antisolvent crystallization of pharmaceutical compounds: Current status and future perspectives," *Drug Delivery and Translational Research*, vol. 13, no. 2, pp. 400–418, 2023, doi: 10.1007/s13346-022-01219-1.

[53] G. Yu et al., "Preparation of daidzein microparticles through liquid antisolvent precipitation under ultrasonication," *Ultrasonics Sonochemistry*, vol. 79, 2021, doi: 10.1016/j.ultsonch.2021.105772.

[54] M. T. D. C. Español et al., "Ultrasound-assisted biomimetic synthesis of MOF-Hap nanocomposite via 10×SBF-like for the photocatalytic degradation of metformin," *Applied Science and Engineering Progress*, vol. 17, no. 2, pp. 1–16, 2024, doi: 10.14416/j.asep.2023.11.002.

[55] Y. Hu et al., "A review on the effect of ultrasonic-assisted curing on the quality of meat products," *Applied Science and Engineering Progress*, vol. 18, no. 2, pp. 1–18, 2025, doi: 10.14416/j.asep.2024.11.006.